J. Phys.: Condens. Matter **9** (1997) 3387–3397. Printed in the UK PII: S0953-8984(97)72259-8

Effects of thermal conduction in sonoluminescence

M-C Chu†‡ and D Leung‡

† Department of Physics, The Chinese University of Hong Kong, Shatin, NT, Hong Kong
‡ W K Kellogg Radiation Laboratory, Caltech 106-38, Pasadena, CA 91125, USA

Received 26 February 1996, in final form 3 October 1996

Abstract. We show by numerical hydrodynamic calculations that there are two important effects of thermal conduction in sonoluminescence: (i) the bubble remains close to being isothermal during the expansion phase; and (ii) a cold, dense layer of air is formed at the bubble wall during the contraction phase. These conclusions are not sensitive to the particular equation of state used, although details of the dynamical evolution of the bubble are.

1. Introduction

Recent advances in techniques for maintaining a stable oscillating air bubble in water using ultrasound fields [1] have led to several remarkable discoveries. Under certain conditions, a narrow and regular flash of light, the width of which is less than 50 ps, is emitted during each cycle of the bubble oscillation [2]. The intensity and the spectra of the emitted light are very sensitive to external parameters such as the water temperature, the intensity of the acoustic fields [3], and the percentage of dissolved noble gas [4]. Such a conversion of sound into light represents a high concentration of energy, and it has been speculated that the pressure and temperature at the centre of the bubble could be high enough to ignite nuclear fusion [5].

To understand the dynamics of the bubble oscillation, hydrodynamic equations for the coupled water–air system in spherical coordinates have been studied using various approximations. Assuming the incompressible limit for water and ignoring the air pressure, Rayleigh obtained the famous Rayleigh equation relating the bubble wall acceleration and velocity to the driving pressure [6]. The equation was modified later by the incorporation of the first-order terms in deviations from the incompressible limit, resulting in the Rayleigh–Plesset (R–P) equation [7]:

$$R\ddot{R} + \frac{3}{2}\dot{R}^2 - \frac{2\dot{R}}{c_w}(R\ddot{R} + \dot{R}^2) = \frac{\Delta P}{\rho} + \frac{R}{\rho c_w}\frac{\mathrm{d}\,\Delta P}{\mathrm{d}t} \tag{1}$$

where R, $\dot{R}$, $\ddot{R}$ are the position, velocity and acceleration of the bubble wall, ρ and c_w the density and speed of sound in the liquid, and $\Delta P \equiv P(R,t) - P_a(t) - P_0$, with $P(R,t)$ the liquid pressure at the bubble wall, $P_a(t)$ the acoustic drive pressure, and P_0 the ambient pressure above the liquid. Applying the R–P equation and the adiabatic approximation for an excluded-volume van der Waals (EVW) gas inside the bubble, i.e., gas pressure, density, and internal energy being spatially uniform, Löfstedt *et al* obtained a description of the bubble dynamics that is fairly accurate for most of a cycle of the oscillation [8]. This model was later refined by Wu and Roberts [5] who solved the hydrodynamic equations for

0953-8984/97/163387+11$19.50

an EVW gas coupled to the motion of the bubble wall approximated by the R–P equation. Non-adiabatic effects in the gas motion were revealed in this calculation. In particular, it was shown that a spherical shock wave could be generated during the contraction phase, and its convergence led to temperature and pressure exceeding 10^7 K and 10^8 atm near the bubble centre. For such conditions, the air in the bubble is expected to be fully ionized, and nuclear fusion is possible. However, at late stages of the bubble collapse, the bubble wall moves at a speed large compared with the speed of sound in water, which violates the assumption of the R–P equation. Also, the EVW equation of state (EOS) becomes unrealistic at high temperature and pressure. A fully coupled air–water hydrodynamic simulation was carried out by Moss *et al* [9] using an EOS that takes into account dissociation and ionization in the gas. While the results differ quantitatively from those of Wu and Roberts, e.g., the maximum temperature reaches only about 10^6 K, the picture in which a converging shock produces high temperature and pressure and the reflected diverging shock quenches them on a picosecond time-scale remains intact.

In this paper we consider the effects of thermal conduction on sonoluminescence. Previous calculations ignoring thermal conduction have shown that a large temperature gradient is created between the gas and the liquid for the major part of the bubble oscillation, making it possible for significant heat flow to occur in the system, which in turn can lead to non-trivial effects on the hydrodynamics. We will show that thermal conduction does indeed produce significant effects on the bubble dynamics.

2. The formulation and method

Assuming local equilibrium and spherical symmetry, the time evolution of the bubble is described by the hydrodynamic equations in spherical coordinates, which express the conservation of mass, momentum, and energy. Since the bubble radius changes by two orders of magnitudes in one cycle, it is convenient to use a Lagrangian scheme in which the grids follow the motion of fluid elements. The mass coordinate is defined by

$$y \equiv \int_{r(0,t)}^{r(y,t)} \rho r^2 \, \mathrm{d}r \tag{2}$$

where r is the position of the mass element and ρ the density. The hydrodynamic equations then simplify to

$$\frac{\partial u}{\partial t} = -r^2 \frac{\partial P}{\partial y} \tag{3}$$

$$\frac{\partial \epsilon}{\partial t} = -P \frac{\partial}{\partial y}(r^2 u) + \frac{\partial}{\partial y}\left(\kappa \rho r^4 \frac{\partial}{\partial y} T\right) \tag{4}$$

where $u \equiv \partial r/\partial t$ is the radial velocity, ϵ is the internal energy, and κ is the thermal conductivity.

We have used three equations of state. At room temperature, air behaves like an EVW gas:

$$\epsilon = (1/\rho - b)P/(\gamma - 1) = C_v T \tag{5}$$

where $b = 0.036$ l m^{-1} is the van der Waals excluded volume, $C_v = 717.65$ J K^{-1} kg^{-1} is the heat capacity of air, and $\gamma = 1.4$ is the adiabatic index. However, at temperatures above 2500 K, dissociation of air molecules becomes important, and at about 8000 K, ionization of the atomic constituents occurs. These processes modify the EOS of air substantially at high temperature. We will also present results using two EOSs taking these into account. The

Srinivasan EOS is a numerical EOS based on curve fits to empirical data [10], and is valid for temperatures up to 25 000 K and densities up to a thousand times normal air density, taking into account dissociation and ionization effects. As we shall see, our calculations often reach temperatures and densities exceeding this range. The Moss EOS [9] represents an attempt to correct for high-pressure effects, which become important at late stages of the bubble contraction. The Moss EOS can be parametrized as

$$P = R'T\rho\,[1 + m_D(1 + 2m)] + \frac{3}{2}E_c\rho_0\tilde{\rho}^2(\tilde{\rho}^2 - 1) \tag{6}$$

$$\epsilon = C_vT\left[1 + \frac{m_D}{5}(1 + 6m)\right] + \frac{R'\theta(1 - m_D)}{e^{\theta}/T - 1} + m_DR'\left[T_D + 2\sum_i m_iT_i\right] + E_c\left[\frac{\tilde{\rho}}{2}(\tilde{\rho}^2 - 3) + 1\right] \tag{7}$$

where $R' = 0.4C_v$ is the gas constant for air,

$$m_k \equiv 0.5\left[\tanh(7T/T_k - 6.3) + \tanh(6.3)\right] \tag{8}$$

$$m \equiv \sum_{i=1}^{5} m_i \tag{9}$$

$$\tilde{\rho} \equiv \rho/\rho_0 \tag{10}$$

and the constants $\rho_0 = 1.113$ g cm^{-3}, $E_c = 2.52 \times 10^9$ erg g^{-1}, $\theta = 3340$ K, $T_D = 9.7$ eV, and $T_i = 14.5,\ 29.6,\ 47.4,\ 77.5$, and 97.5 eV for $i = 1$ to 5. For density above about 1 g cm^{-3}, the Moss EOS is much stiffer than the Srinivasan EOS. At low temperature and density, the three EOSs exhibit only negligible differences. We therefore use the EVW EOS until a temperature and a density are reached for which the EOSs begin to differ from each other. We will show that whereas the three EOSs lead to quantitatively different results, our qualitative conclusions on the effects of thermal conduction hold independently of the EOS.

We also need to specify the boundary conditions. At the centre of the bubble, by symmetry,

$$u(r = 0) = 0 \tag{11}$$

$$\partial_r T(r = 0) = 0. \tag{12}$$

At the bubble wall, the pressure is discontinuous. Using the subscripts l and g for liquid and gas respectively, we have

$$P_l(R, t) = P_g(R, t) - 2\sigma/R - 4\nu\dot{R}/R \tag{13}$$

where ν is the shear viscosity of the liquid, and σ is the surface tension coefficient. The heat flux on the other hand is continuous:

$$\kappa_g\,\partial_r T|_{r=R-\delta} = \kappa_l\,\partial_r T|_{r=R+\delta} \qquad \text{as } \delta \to 0. \tag{14}$$

Since κ_l is usually much greater than κ_g, the temperature gradient in the liquid is much smaller than that in the gas. We therefore neglect the temperature change in the liquid, which is small compared to that in the gas:

$$T(r = R, t) \approx T(r > R, t) \approx T_i \tag{15}$$

where T_i is the initial temperature in the liquid. We have checked that the thermal flux leaking out from the bubble in our calculations would indeed only heat up the thermal layer

immediately next to the bubble wall by just a few degrees Kelvin. Finally, the pressure in the liquid far from the bubble is given by

$$P(r = \infty) = P_a(t) + P_0 \tag{16}$$

with the acoustic drive pressure $P_a(t) = -P_a \sin(\omega_a t)$.

When $\dot{R} \ll c_w$, one can take the R–P approximation to the bubble wall motion. We thus coupled the R–P equation, equation (1), to the hydrodynamic equations for the gas inside the bubble, equations (3) and (4). We used a Lax–Wendroff finite-differencing scheme, together with a generalized version of the artificial viscosity appropriate for spherical coordinates [11]. The bubble was divided into 200 equal-mass shells, and the time step was varied depending on the velocities of the gas, with a maximum time resolution of 10^{-6} ps. In one case, we also carried out the calculation with 400 mass shells; the good agreement between it and the results obtained using 200 mass shells gives some confidence as regards the convergence of our results. Overall energy conservation is observed to within a few per cent in our calculations.

There are two obvious shortfalls in our method: the use of artificial viscosity smears out shock fronts leading to an inaccurate representation of them, and the assumption of the R–P equation breaks down when the bubble wall velocity becomes large compared to the speed of sound in water. Consequently, our results should only be considered semi-quantitative. For example, the maximum temperature depends sensitively on the details of the shock fronts as well as the EOS. However, we believe that our conclusions, which are based on results from the hydrodynamic regime when the motion of the bubble wall is subsonic and our method is adequate, are sound.

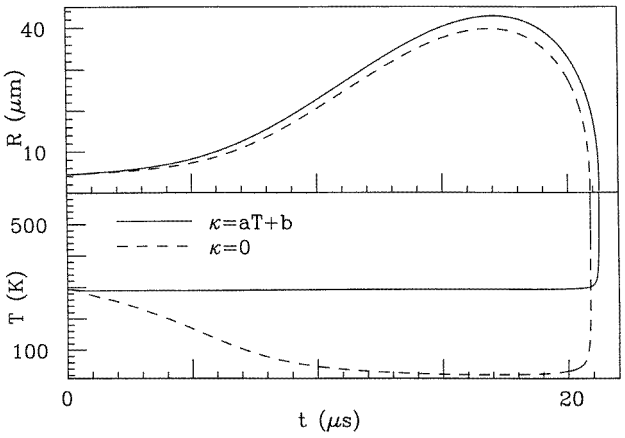

Figure 1. The calculated bubble radius R and the temperature at the centre (T) versus time, for a bubble of an EVW gas with initial conditions $R_i = 4.5$ μm, $T_i = 293$ K, and $P_i = 1$ atm, driven with a sound intensity of $P_a = 1.3$ atm at a frequency of $\omega_a = 26.5$ kHz. The R–P equation is assumed for the bubble wall motion. Results obtained using a thermal conductivity $\kappa = aT + b$ (solid lines) are compared with results obtained with $\kappa = 0$ (dashed lines).

3. Results

We present results for three sets of initial conditions: $T_i = 275, 293, 307$ K, $R_i = 4, 4.5, 5.5$ μm, and $P_a = 1.4, 1.3, 1.25$ atm respectively, and we compared the results

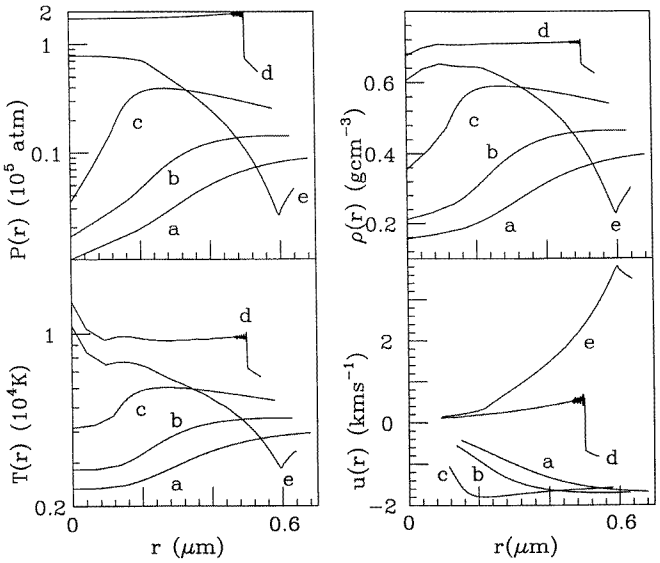

Figure 2. Snapshots of the spatial profiles of the temperature, pressure, velocity, and density at five succeeding instances (labelled from a to e) separated by equal intervals of 4.5 ps, beginning at $t_a = 21.252\,306$ μs, when the thermal conductivity was turned on: $\kappa = aT + b$. See figure 1 for the input parameters. An EVW EOS was used for the gas.

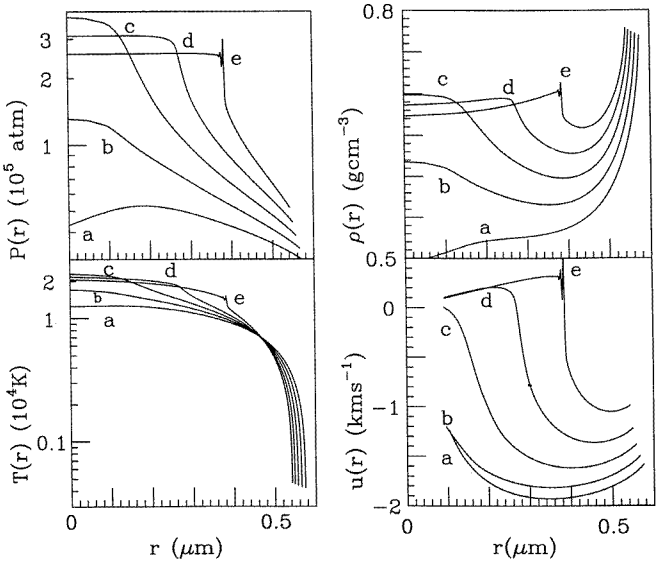

Figure 3. As figure 2, but for $\kappa = 0$. The profiles are separated by equal intervals of 30 ps, beginning at $t_a = 20.893\,665$ μs.

with and without thermal conduction to study its effects. We took $\omega_a = 26.5$ kHz, $\nu = 0.007$ kg m^{-1} s^{-1}, $P_0 = 1$ atm, and $\sigma = 0$. Our calculation is similar in spirit to that of Hickling [12], who studied the effects of thermal conduction in the initial bubble collapse; we calculated through a complete cycle of the bubble motion. We differ from

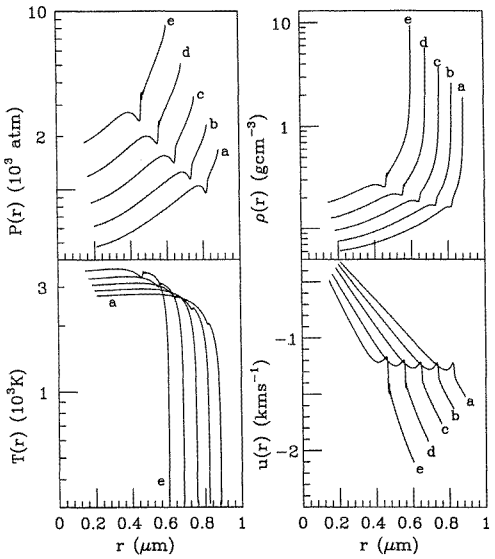

Figure 4. As figure 2, but for the Srinivasan EOS for the gas (see the text). The lines labelled a to e are snapshots at succeeding times at 40 ps intervals beginning at $t = 21.252\,12$ μs.

Kamath *et al* [13] in that we do not assume the pressure to be uniform.

The details of the bubble dynamics are presented in figures 1–5 taking the initial conditions $T_i, R_i = 293$ K, and 4.5 μm. We show in figure 1 the time evolution of the bubble radius R and temperature at the centre of the bubble, assuming an EVW EOS. The solid lines indicate results obtained with a thermal conductivity [14] $\kappa = aT + b$, where $a = 5.28$ erg cm^{-1} s^{-1} K^{-2} and $b = 1165$ erg cm^{-1} s^{-1} K^{-1}, which is a good approximation for air up to about 3000 K. The dashed lines represent the results with the thermal conduction turned off. Whereas thermal conduction has only a small effect on the bubble radius (top panel), it affects the temperature inside the bubble significantly. When the bubble expands, its interior is colder than the surrounding liquid, and heat is absorbed *into* the bubble if thermal conduction is allowed. As a result, the temperature in the bubble is kept close to the water temperature, in agreement with a linear analysis [15]. If the thermal conduction is turned off on the other hand, the bubble interior becomes very cold and the pressure very low throughout the expansion phase. The conditions of the bubble at the beginning of the contraction phase are therefore drastically changed as a result of thermal conduction.

When the bubble contracts, its interior heats up rapidly. We plotted the profiles of the temperature, pressure, velocity, and density in the bubble with (figure 2) and without (figure 3) thermal conduction at instances around maximum compression. A comparison of the density and temperature profiles shows that thermal conduction leads to the formation of a cold, dense layer of air at the bubble wall. This is a result of the fact that thermal conduction keeps the bubble wall cold ($\approx T_i$), but the pressure there is high during contraction, so the air density becomes very high, reaching close to the maximum value allowed in the EOS. This dense layer of air remains cooled at the bubble wall throughout most of the contraction phase, leaving relatively dilute gas at the centre of the bubble. Even though some heat leaks out from the bubble, the fact that fewer air molecules share the kinetic energy converted from the $P\,\mathrm{d}V$ work means that a high temperature is still reached

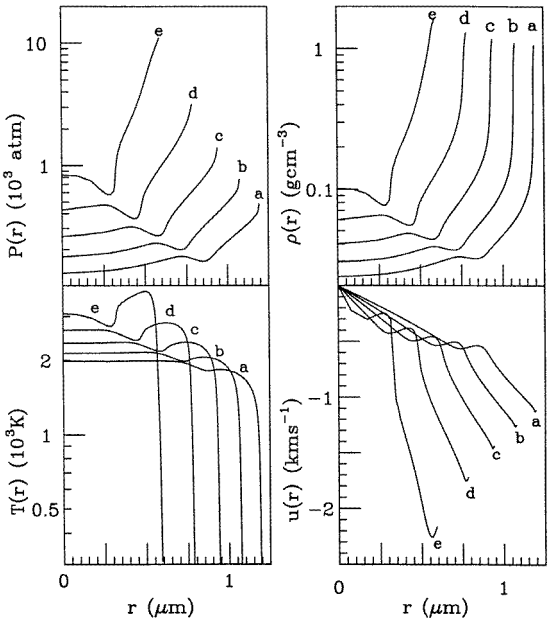

Figure 5. As figure 2, but for the Moss EOS for the gas (see the text). The lines labelled a to e are snapshots at succeeding times at 10 ps intervals beginning at $t = 21.2519$ μs.

near the bubble centre. When the pressure at the centre becomes so high that the gas at the core rebounds against the infalling outer shells (shown from c to e), a diverging shock front develops, which quenches the temperature at the centre rapidly.

In figure 4, we show the profiles at an early stage of the contraction phase when we substituted the Srinivasan EOS for the EVW EOS for air starting at $t = 21.25$ μs, when the maximum temperature inside the bubble is about 1200 K. The converging shock tends to push up the temperature, but that is offset by ionization and dissociation effects which produce more degrees of freedom. A dense layer of air is again formed at the bubble wall throughout the contraction phase. The minimum bubble radius is about 0.14 μm (not shown in the figure)—much less than that with an EVW gas, of about 0.54 μm. This is a result of the fact that the Srinivasan EOS is softer at high density, making it possible to squeeze the bubble to a smaller volume. The gas density therefore reaches an extraordinarily high value, exceeding 100 g cm^{-3} near the bubble wall. This is of course an unphysical result based on an extrapolation of the Srinivasan EOS to a regime where it is not valid. It is likely that the gas would undergo some phase transitions well before reaching such a density, and the bubble dynamics could be affected significantly.

As expected, when the Moss EOS is used (starting at $t = 21.24$ μs, maximum $T < 600$ K), the profiles change quantitatively (see figure 5). The minimum bubble radius and maximum density are intermediate between those obtained from the other two EOSs, which corresponds with the fact that the Moss EOS is intermediate in stiffness between the Srinivasan and the EVW EOSs at high density. The picture in which a cold dense layer of air is formed at the bubble wall still holds, with the density there reaching several times that of water. We again caution that some phase transitions probably occur and modify the dynamics, but these are not included in the EOS.

Both the expansion ratio $r_e \equiv R_{\max}/R_{\text{init}}$, $R_{\max}$ and R_{init} being the maximum and the

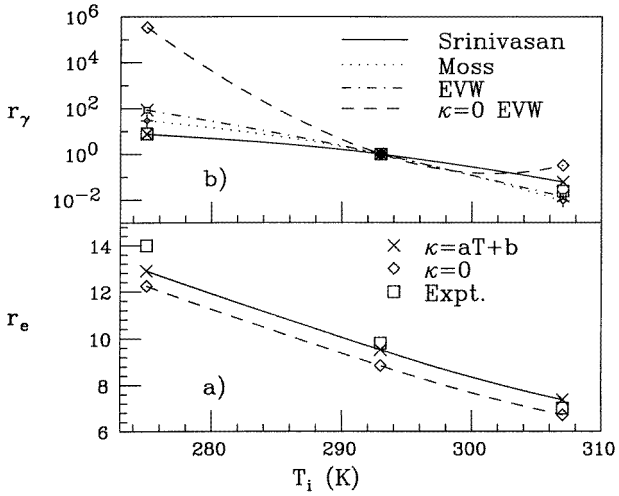

Figure 6. The expansion ratio and photon emission intensity for $T_i = 275, 293, 307$ K, compared with experimental data (squares). Results obtained using an EVW EOS with (stars) and without (diamonds) thermal conduction are shown together with two more realistic EOSs with thermal conduction (crosses: the Srinivasan EOS; daggers: the Moss EOS). The lines are drawn in to guide the eyes only. In (a) the expansion ratios $R_{\max}/R_{\text{init}}$ are shown. In (b) the numbers of photons per burst I scaled to that at $T_i = 293$ K are plotted. For the calculations, black-body radiation was assumed.

equilibrium bubble radii, and the photon emission intensity are known to be sensitive to the water temperature [3]. We compare our results with the data in figure 6, for three water temperatures: $T_i = 275, 293, 307$ K. We show the expansion ratio, r_e, comparing the results obtained with (crosses) and without (diamonds) thermal conduction, to experimental data (squares) taken from reference [3]. Throughout the expansion phase, the EVW EOS is a good approximation, and there are negligible differences in the expansion ratio between the three EOSs. Thermal conduction has a small but noticeable effect on r_e: because the bubble interior is warmer during the expansion phase, the air pressure is higher and the expansion ratio larger. Results with thermal conduction are closer to the data, although there seems to be a deficiency at $T_i = 275$ K.

We have also observed a sensitive dependence of the maximum temperature in the interior of the bubble on the water temperature, much of this dependence arising from the fact that the ambient radius R_{init} is sensitive to T_i. If we assume a thermal emission mechanism and scale the emitted light intensity with $T^4_{\max}$, we obtain a water temperature dependence of the light intensity in fair agreement with experimental data. However, we caution readers that the maximum temperature calculated in this way, which depends sensitively on the detailed dynamics of the shock fronts as well as the EOS, may not be accurate enough.

In figure 6(b), we plot the observed number of photons per burst normalized to that at $T_i = 293$ K (squares), and we compare these with the calculated ratio of the maximum photon intensities assuming black-body radiation:

$$r_\gamma = T^4_{\max}(T_i)/T^4_{\max}(T_i = 293\ \text{K}). \tag{17}$$

We assume that the ratio of the photon intensity at different T_is reflects to a large extent the ratio of the maximum temperatures in the bubble interior, i.e., numerical factors resulting from the space-time integration of the emission probability with the detection efficiency

folded in roughly cancel in these ratios. It is possible that the photon intensity may measure the surface temperature of a hot core instead of the maximum temperature. Such a crude comparison only serves as a rough indication of the effects of thermal conduction. Results obtained with the EVW EOS and thermal conduction ignored are indicated by diamonds, and these clearly disagree with the data. Incorporation of thermal conduction brings the results (stars connected by a dashed line) closer to the data, and the use of the Srinivasan EOS (crosses connected by a solid line) as well as the Moss EOS (daggers connected by dots) improves it further. Here again, results obtained using the Moss EOS are intermediate between the EVW and the Srinivasan EOSs. The maximum temperature reached is sensitive to the stiffness of the EOS; the stiffer the gas is, the higher the temperature at the interior of the bubble gets.

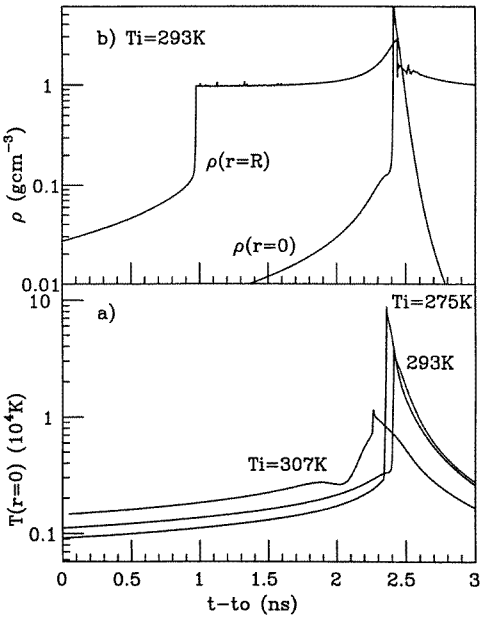

Figure 7. The time history of (a) the temperature near the bubble centre, $T(r = 0)$, and (b) the density near the bubble centre, $\rho(r = 0)$, compared with that at the bubble wall, $\rho(r = R)$. Results for three initial water temperatures $T_i = 275, 293, 307$ K, are shown in (a), with the starting time t_0 chosen for each T_i so that they fit into this 3 ns window around the time of maximum compression. In (b), only the results for $T_i = 293$ K are shown. The Moss EOS is used.

In figure 7, we plot the time history of the temperature near the centre of the bubble (figure 7(a)) and also compare the density near the bubble wall ($\rho(r = R)$) to that near the centre ($\rho(r = 0)$) for a 3 ns window around the time of maximum compression. The Moss EOS is assumed, and the starting time t_0 is chosen for each T_i so that the curves for all three T_is fit into the window in figure 7(a). Only the density for $T_i = 293$ K is shown in figure 7(b), because the other two cases are very similar. As shown clearly in figure 7(b), the density at the bubble wall jumps to a density comparable to that of water at about 1.4 ns before the temperature at the bubble centre surges to a maximum. For about 1.4 ns after $t - t_0 = 1$ ns, the density near the bubble wall remains relatively constant and much higher than near the centre, until the shock front converges at the centre, giving rise

to a rapid surge in the temperature and density there. This pulse of temperature and density takes a rather asymmetric shape: the rise is very fast, followed by a slower relaxation. The behaviour of $\rho(r = R)$ is rather sensitive to the particular EOS used. Here, the specific value of the relatively constant density is given by that of a solid lattice frozen under high pressure. The Moss EOS becomes stiffer after reaching this density, leading to a much slower rise in $\rho(r = R)$. Figure 7 suggests strongly that the layer of air near the bubble wall undergoes a phase transition at $t - t_0 = 1$ ns, solidifying into a rigid lattice.

4. Summary

We have solved the hydrodynamic equations describing the motion of the gas in a bubble in an almost incompressible fluid. Thermal conduction was included in our calculations, and it has two important effects on the bubble dynamics: (i) the bubble remains close to being isothermal during the expansion phase; and (ii) a cold, dense layer of air is formed at the bubble wall during the contraction phase. These effects, as well as the picture in which a converging shock is generated during the contraction, heating up the air inside the bubble, and the reflected shock quenches the temperature quickly, are not sensitive to the particular EOS used, although the details are.

The present hydrodynamic calculations all show the remarkable range of temperature, density, and pressure reached in a sonoluminescing bubble. Future investigation of the detailed bubble dynamics will rely critically on a better knowledge of the EOS at high temperature and pressure. Possible deviations from spherical symmetry during a cycle of the bubble oscillation will also need to studied. Properties of the air–water interface may also be important governors of sonoluminescence characteristics and warrant careful study. Other transport processes such as radiation should also be incorporated into a full hydrodynamic treatment of the problem [16].

Acknowledgments

We thank Professor Steve Koonin and Tom Tombrello for stimulating discussions. We thank Professor Joseph Shepherd for discussions and comments on the manuscript, as well as providing us with the numerical Srinivasan EOS for air. We also thank Dr William Moss for useful discussions regarding the EOS. This research was partially supported by an RGC Earmarked Grant CUHK312/96P, a Chinese University Direct Grant 702/1, and the US National Science Foundation under grants PHY90-13248 and PHY94-12818 at Caltech. DL gratefully acknowledges the support of the Caltech SURF program.

References

[1] Gaitan D F, Crum L A, Church C C and Roy R A 1992 *J. Acoust. Soc. Am.* **91** 3166
[2] Barber B P and Putterman S J 1991 *Nature* **352** 318
Barber B P, Hiller R, Arisaka K, Fetterman H and Putterman S J 1992 *J. Acoust. Soc. Am.* **91** 3061
Hiller R, Putterman S J and Barber B P 1992 *Phys. Rev. Lett.* **69** 1182
[3] Barber B P, Wu C C, Lofstedt R, Roberts P H and Putterman S J 1994 *Phys. Rev. Lett.* **72** 1380
[4] Hiller R, Weninger K, Putterman S J and Barber B P 1994 *Science* **266** 248
[5] Wu C C and Roberts P H 1993 *Phys. Rev. Lett.* **70** 3424
[6] Rayleigh Lord 1917 *Phil. Mag.* **34** 94
[7] Plesset M 1949 *J. Appl. Mech.* **16** 277
Noltingk B and Neppiras E 1950 *Proc. Phys. Soc.* B **63** 674
Keller J and Miksis M 1980 *J. Acoust. Soc. Am.* **68** 628

Prosperetti A 1984 *Rend. SIF* **XCIII** 145
[8] Löfstedt R, Barber B P and Putterman S J 1993 *Phys. Fluids* A **5** 2911
[9] Moss W C, Clarke D B, White J W and Young D A 1994 *Phys. Fluids* **6** 2979
[10] Srinivasan S, Tannehill J C and Weilmuenster K J 1987 *Simplified Curve Fits for the Thermodynamic Properties of Equilibrium Air (NASA Reference Publication 1181)*
[11] Benz W 1991 *Late Stages of Stellar Evolution. Computational Methods in Astrophysical Hydrodynamics (Springer Lecture Notes in Physics 373)* ed C B de Loore (Berlin: Springer) p 259
Richtmyer R D and Morton K W 1957 *Difference Methods for Initial Value Problems* (New York: Interscience)
[12] Hickling R 1963 *J. Acoust. Soc. Am.* **35** 967
[13] Kamath V, Prosperetti A and Egolfopoulos F N 1993 *J. Acoust. Soc. Am.* **94** 248
[14] Prosperetti A, Crum L A and Commander K W 1988 *J. Acoust. Soc. Am.* **83** 502
[15] Plesset M S and Hsieh D-Y 1960 *Phys. Fluids* **3** 882
[16] Kondic L, Gersten J I and Yuan Chi 1995 *Phys. Rev.* E **52** 4976